



CHANGE IN DYNAMIC CHARACTERISTICS OF BASE-ISOLATED BUILDINGS WITH IRREGULAR SHAPE BASED ON LONG-TERM VIBRATION RECORDS

Katsuaki KONNO¹ and Masami TOYODA²

¹ Member, Dr. Eng., Shibaura Institute of Technology,
Tokyo, Japan, konno@sic.shibaura-it.ac.jp

² Central Japan Railway Company,
Tokyo, Japan

ABSTRACT: Long-term structural health monitoring is conducted on the Toyosu campus of Shibaura Institute of Technology. The buildings are installed with accelerometer sensors and incorporated with base isolation devices, which are also installed in the ground. The fast Fourier transform (FFT) was used to analyze the microtremor records for nine years. The result shows a negative correlation between temperature and the natural period of the buildings, and the periods have increased by approximately 5% since the 2011 off the Pacific coast of Tohoku Earthquake. The auto-regressive exogenous (ARX) model was used to analyze the earthquake records. The result shows that the natural period and damping ratio of buildings are dependent on the amplitude of vibration. The periods have increased by 6%–10% due to the abovementioned earthquake, but the damping ratios have not changed.

Keywords: *Long-term monitoring, Dynamic characteristics, ARX model, Base-isolated building, Irregular shaped building*

1. INTRODUCTION

The evaluation of structural health is important for maintenance management and for the understanding of and response to seismic functions immediately after an earthquake. For this reason, structural health monitoring based on seismic observations has been conducted in many cases (e.g., Okamoto et al.¹). Observation records are classified into inputs (e.g., earthquake motion) and outputs (structural response) that act on the structure, and the vibration characteristics of the structure (e.g., natural period, damping ratio) are estimated based on system identification theory. Changes in these estimated values are correlated with deterioration and damage at the layer and member level to evaluate structural health².

In structural health monitoring, not only seismic records but also microtremor records can be used by employing high-sensitivity sensors. The use of microtremors allows continuous monitoring of changes in the vibration characteristics of the structure. For example, Okamoto et al.¹ and Hatayama et al.³ monitored a super high-rise steel structure building and a three-story steel structure building,

respectively, using microtremor and seismic records. They reported that the natural frequencies showed seasonal variations and that there was a positive correlation between the natural frequencies and air temperature. On the contrary, Saito⁴⁾ reported a negative correlation between natural frequencies and air temperature for a six-story steel structure building with column-head isolation composed of lead-plugged laminated rubber. The reason for this correlation is not mentioned; however, it is assumed that the rubber and lead softened as the temperature rose, lowering the natural frequency of this column-head base isolation system since it is exposed to the surrounding air. Therefore, with this exception, the positive correlation between natural frequencies and air temperature can be considered a general characteristic of steel structure and reinforced concrete buildings⁵⁾. To accurately extract changes in structural health monitoring over time, it is necessary to understand this seasonal component, and it is important to understand the mechanism of the relationship between changes in natural frequencies and temperature. A mechanism of reinforced concrete buildings is examined in a thermal stress test of concrete test columns by Kanazawa⁵⁾. The results show that when one side of the test column is heated, a temperature difference is generated in the cross section, increasing the stiffness of the concrete member and thus increasing the natural frequency. Alternatively, when the entire column is heated, the temperature difference in the cross section disappears, decreasing the stiffness due to the softening of the concrete material and thus decreasing the natural frequency. However, this mechanism cannot be explained for steel structure building. To the best of the authors' knowledge, no empirical investigations have been conducted on the mechanism in steel structure buildings. Although the mechanism has not been investigated in this report, it should be noted that concrete in steel tubes may also be involved since the subject buildings are concrete-filled steel tube (CFT) structures.

In the structural health monitoring of microtremors in steel structure buildings, a case of natural frequency change to the low frequency side after the 2011 off the Pacific coast of Tohoku Earthquake (hereinafter referred to as "Tohoku Earthquake") has been reported⁴⁾. Structural health monitoring using microtremors allows continuous monitoring of the condition of a structure. However, the information obtained is only about the vibration characteristics at small amplitudes, so it may be difficult to determine the seismic function during strong earthquakes. In this respect, albeit intermittently, seismic records provide information on vibration characteristics during strong earthquakes. In the case of the application to seismic records of steel structure buildings, it is reported⁶⁾⁻⁸⁾ that the natural frequency and damping ratio show amplitude dependence. That is, the amplitude dependence of the natural frequency changes to the low frequency side when a large amplitude is experienced, and the amplitude dependence of the damping ratio does not clearly change before and after a large amplitude is experienced.

This study focuses on two CFT medium-rise buildings (multi-activity building and classroom building) with large aspect ratios and a CFT high-rise building (research building) connected to one of the two buildings in an L shape. These three buildings are extremely irregular shaped buildings. Seismic isolators are located at different heights even within the same building, and a piloti is found in the high-rise building⁹⁾. To understand the dynamic behavior of complex structures, multiple accelerometers were installed on the three buildings and in the ground to observe the vibration over a long period of time. In the 2011 off the Pacific coast of Tohoku Earthquake, approximately 300 cm/s² was observed on the top floor of the classroom building, and cracks were observed in the nonstructural members such as interior materials. Siringoringo and Fujino¹⁰⁾ used seismic records from September 2010 to December 2012 for the two connected buildings mentioned above to show that the natural frequencies dropped significantly during the Tohoku Earthquake and recovered, although not back to the levels prior to the earthquake. The damping ratios increased significantly during the Tohoku Earthquake, but the trend of amplitude dependence was almost the same before and after Tohoku Earthquake. The trend in the amplitude dependence of the natural frequencies and damping ratios is the same as in the previous studies⁶⁾⁻⁸⁾.

In this study, the natural period was identified from the microtremor records, and the natural period and damping ratio were identified from seismic records. Moreover, their changes over time and dependence on amplitude were investigated. This article differs from reference 10 in that it uses microtremor records to identify the natural period, all three buildings are included in the analysis, and

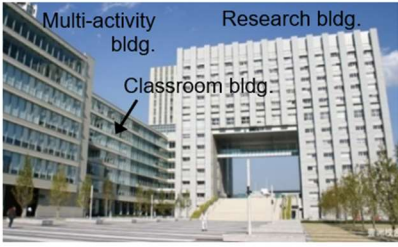


Photo 1 Toyosu Campus of Shibaura Institute of Technology

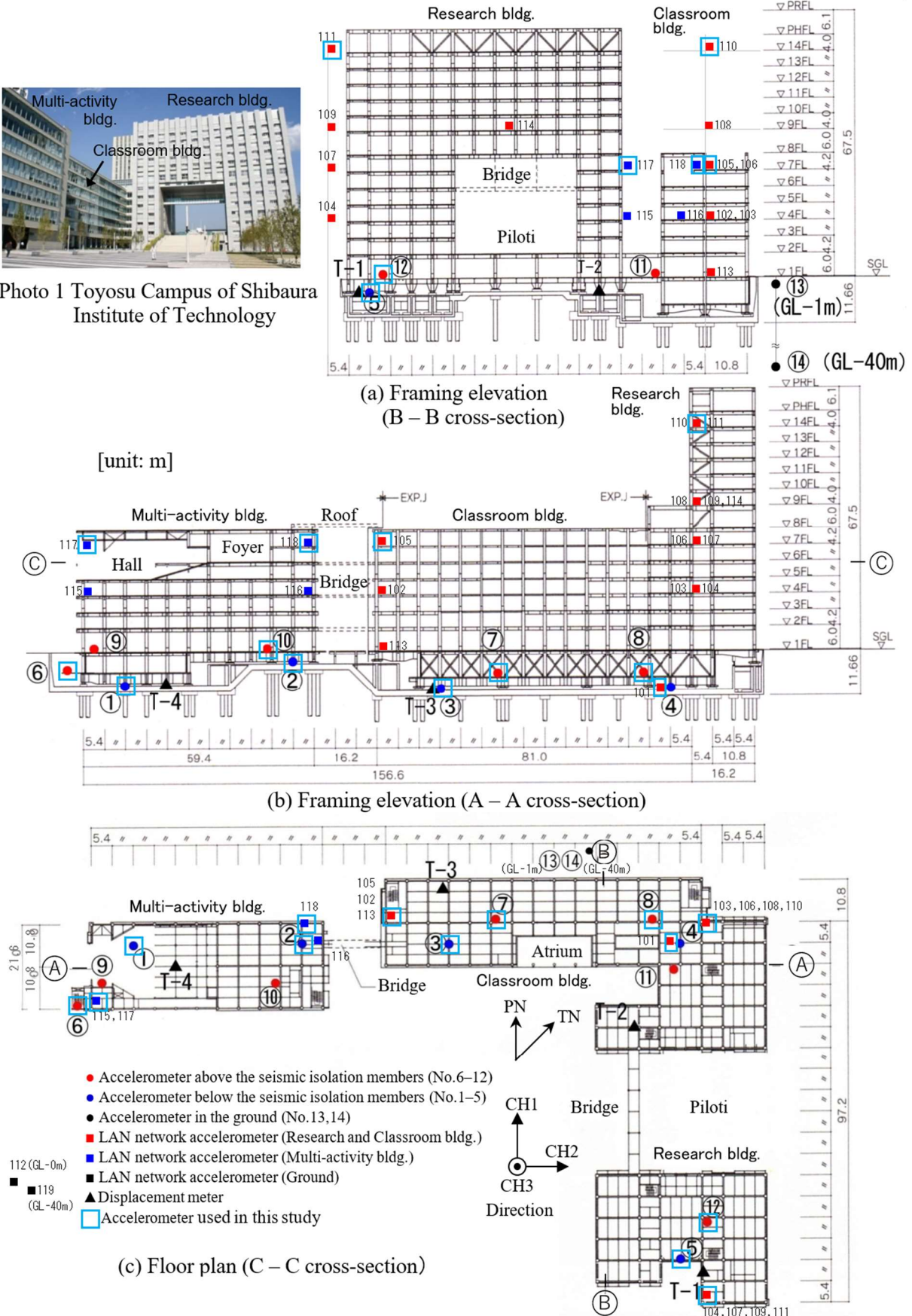


Fig. 1 Framing elevation and floor plan of Toyosu school building and seismic instrument location¹¹⁾

seismic records from January 2013 to February 2020 are additionally used. Now that the Nankai Trough earthquake and the Tokyo Metropolitan earthquake are expected to occur, the subject structures may experience large amplitudes that exceed those of the Tohoku Earthquake. Although the buildings have a unique shape and configuration, it is possible that similar structures will be constructed in the future. Therefore, this article is intended to serve as a reference work and describes the obtained data and other information in as much detail as possible.

2. SUMMARY OF SUBJECT BUILDINGS⁹⁾

The construction of the subject structures (Photo 1) was completed in September 2005, and the school opened in April 2006. As shown in Fig. 1, the school building consists of three buildings: a seven-story multi-activity building, a classroom building, and a 14-story research building. As shown in Fig. 1(c), the angle between the long or short side of the building and true north is approximately 45°, but for the sake of simplicity, the orientation of the building will be described based on plant north in this article. The superstructures of all three buildings are steel construction with CFT columns. The classroom and research buildings are jointed up to the seventh floor, while the second to seventh floors of the research building have a piloti, making it a structurally complex, irregular shaped (L-shaped) building. Conversely, the superstructures of the multi-activity and the classroom buildings are separated. A connecting bridge with sliding and rotating mechanisms is installed between the second, fourth, and sixth floors of the two buildings to release the relative displacement between the buildings.

Seismic isolation layers are located between the superstructures and the foundation slabs. Four types of isolation components (laminated rubber isolators, laminated rubber isolators with U-shaped steel dampers, lead dampers, and elastic sliding bearings) are placed within the seismic isolation layer. As shown in Fig. 1(a) and (b), the foundation slab is continuous but becomes shallower near the boundary between the multi-activity and classroom buildings and on the lower side of the piloti of the research building. The thickness of the foundation slab is only 100 cm in the lower area of the piloti of the research building, while the rest is 150 cm. The thickness of the floor slab directly above the seismic isolators is 20 cm for all three buildings. As shown in Fig. 1(a) and (b), the seismic isolation members are installed at a lower height on the west side of the multi-activity and classroom buildings and at a higher height on the east side of the multi-activity and research buildings. In the research building, the space between the foundation slab and the seismic isolation members (see Fig. 1(a)), except for the lower part of the piloti, is used as a rainwater storage facility. It is structurally constructed between the seismic isolation members and the pile heads, with RC columns of 200–310 cm in length and RC walls of 40–60 cm in thickness between them. From the above, the stiffness of the substructure below the seismic isolation members is considered to be relatively high.

3. OVERVIEW OF THE EARTHQUAKE OBSERVATION SYSTEM¹²⁾

Table 1 presents an overview of the seismic observation system. As shown in Fig. 1, seismographs 1–14 were installed at the time of construction in 2005 to investigate the effectiveness and performance of the seismic isolation members on a soft ground. Five seismographs were installed on the foundation slab below the seismic isolation members, seven seismographs were installed on the first basement floor and the first ground floor, and two seismometers at 1 m and 40 m depth of the ground. These seismometers are servo accelerometers. The waveform data from each accelerometer is sent via a dedicated cable to a CompactFlash (CF) card recorder in the Disaster Prevention Center located on the first floor of the classroom building, where it is recorded at 100 Hz sampling. The recording device uses a GPS clock synchronization.

As shown in Fig. 1, seismographs 101–119 were installed around the superstructures from 2010 to 2013 to investigate the behavior of the superstructures. These seismographs are servo local area network accelerometers, which perform continuous and triggered observations and record acceleration at 100-Hz sampling. A Network Time Protocol (NTP) server incorporated with a GPS clock is used to

perform time synchronization of each accelerometer¹³).

4. CHANGE OVER TIME OF NATURAL PERIOD OF EACH BUILDING USING LONG-TERM MICROTREMOR RECORDS

Continuous observation of microtremors in the buildings is mainly conducted on the fourth floor and above and at two other locations, namely, on the foundation (seismograph 101) and on the first floor of the west side of the classroom building (seismograph 113). Therefore, the natural period was estimated not from the transfer function that requires input/output records but from spectral analysis of long-term microtremor records from the seismographs installed on the top floor corners of each building. Therefore, it should be noted that the natural period presented in this article is the natural period of the building, including the effect of the ground. Table 2 lists the seismographs used to estimate the natural period. The microtremor record consists of a single file of three-component, 10-min acceleration records. A total of 144 files are recorded per day on a memory card in the seismograph. The continuous record keeping started on March 1, 2011, for seismographs 105, 110, and 111, and on May 13, 2012, for seismographs 117 and 118. The procedure for estimating the natural period is as follows:

1. From the 10-min recordings, the waveform data were divided into six windows of 163.84 s with 50% overlap. FFT and a Parzen window with a bandwidth of 0.2 Hz were used to calculate the spectrum of each window. The 10-min spectrum was estimated from the geometric mean spectra for the spectra.
2. The peak period is the period of the largest peak within the period range presented in Table 2 for a 10-min spectrum peak, and the mode frequency among the 144 peak periods for 1 day is the intrinsic period for that day. Rather than average, mode is used to exclude the effects of sudden disturbances, such as earthquakes and strong winds, as much as possible.

Figure 2 shows a spectrum normalized by the maximum value of the period range in Table 2. In all cases, microtremors during the 10-min period from 14:00 on the date indicated in the figure were used, but the earthquake motion was not included. The vertical lines in the figure indicate the location of the peak period of each spectrum. In the classroom and research buildings, the peak period clearly increased after the Tohoku Earthquake.

The estimated natural period is considered to represent the condition of the structure on each day. In terms of maintenance, it is thought that it is easier to use the intrinsic period of each day compared with the average value over some period. In this article, the 10-day average of the natural periods is obtained separately for the beginning (1–10 days), middle (11–20 days), and end (21 days to the end of the month) of each month. In the following, the 10-day average of the natural period is sometimes referred to simply as the natural period. The graphs on the left side of Fig. 3 show the changes of the 10-day average of the natural periods over time for the multi-activity building for approximately 8 years and for the classroom and research buildings for 9 years. Clear seasonal variations are found in the direction of CH1 on the west and east sides of the multi-activity building, CH1 on the north side of the research building, and CH1 and CH2 on the south side of the research building. Figure 3 also shows the 10-day averages of temperature¹⁴) at the Japan Meteorological Agency (JMA) Edogawa seaside station (approximately 7 km east–southeast of the subject structure), indicating that the natural period tends to shorten as the average temperature increases. Therefore, the same trend was observed in these buildings as in previous studies^{1), 3)}. The graphs on the right side of Fig. 3 show the relationship between the average temperature and the natural period. The natural period for the direction of the abovementioned location becomes shorter when the average temperature exceeds 15°–20°. The temperature above 15°–20° corresponds to the room temperature inside the building, which is almost constant throughout the year. When the outside temperature exceeds this temperature, a temperature difference is generated within the members, increasing the rigidity of the entire structure⁵⁾. This is thought to be the reason for the shortening of the natural period. However, the fact that the

Table 1 Overview of earthquake observation system

Seismometer No.	Sensor type	Recorder	Data record	Start date
001-012	Servo Accelerometer (SV-355T)	SAMTAC-700	- Trigger	2005/07/29
013-014	Servo Accelerometer (SA-355CT)			
101-112*	Servo Accelerometer (CV-374A)	Combined unit	- Trigger - Continuous	2010/03/25
113-114, 116-118				2012/05/13
115				2013/03/01
119*	Servo Accelerometer (AS-303D3BH)	CV-374AR		2012/10/26

*: Observations for seismographs 112 and 119 were terminated on December 3, 2019, due to the construction of a new building.

Table 2 Seismometer used to estimate natural period and search range of peak period

Installation Position	Multi-activity bldg. West side / Top flr.	Multi-activity bldg. East side / Top flr.	Classroom bldg. West side/Top flr.	Research bldg. North side/Top flr.	Research bldg. South side/Top flr.
Seismometer No.	117	118	105	110	111
Search range (s)	0.6 – 6.0	0.6 – 6.0	0.6 – 6.0	1.0 – 6.0	1.3 – 6.0

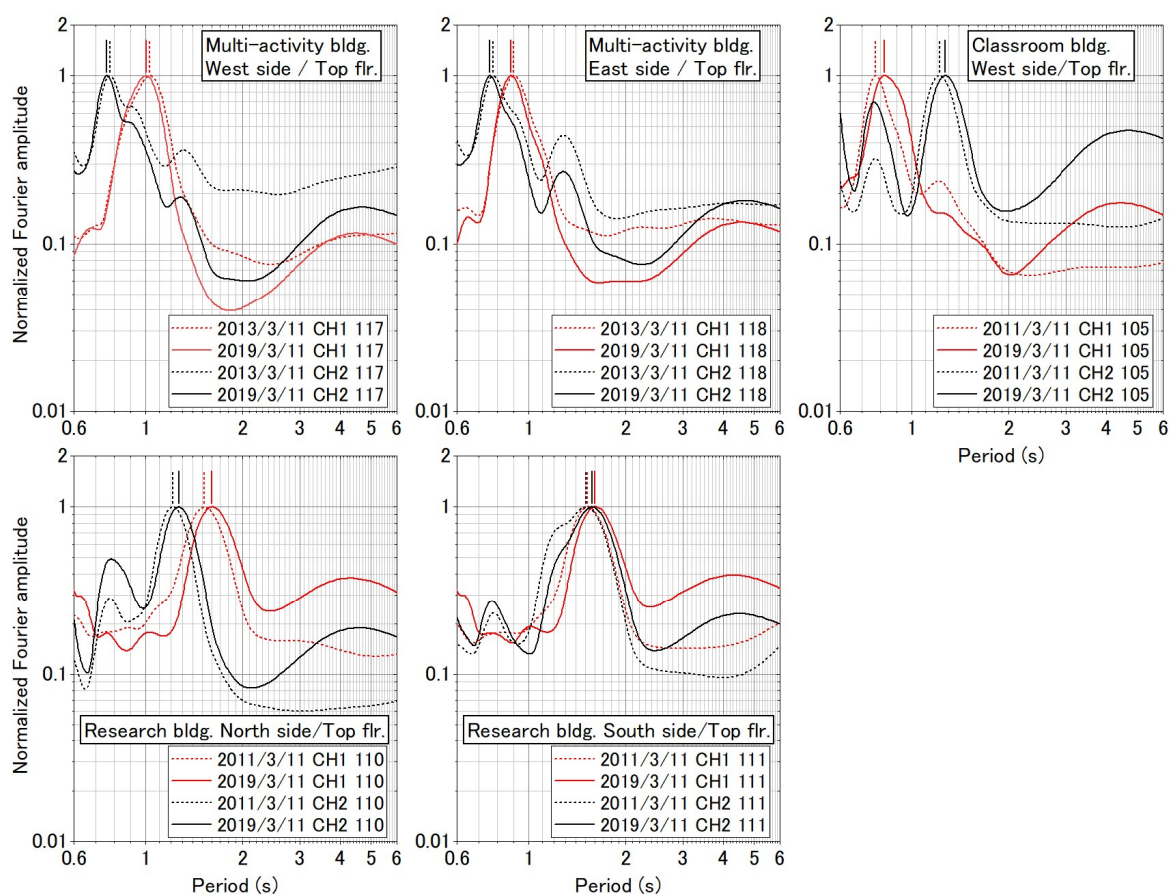


Fig. 2 Normalized spectra of the microtremors on the top floor of each building (10-min records from 14:00 were used.)

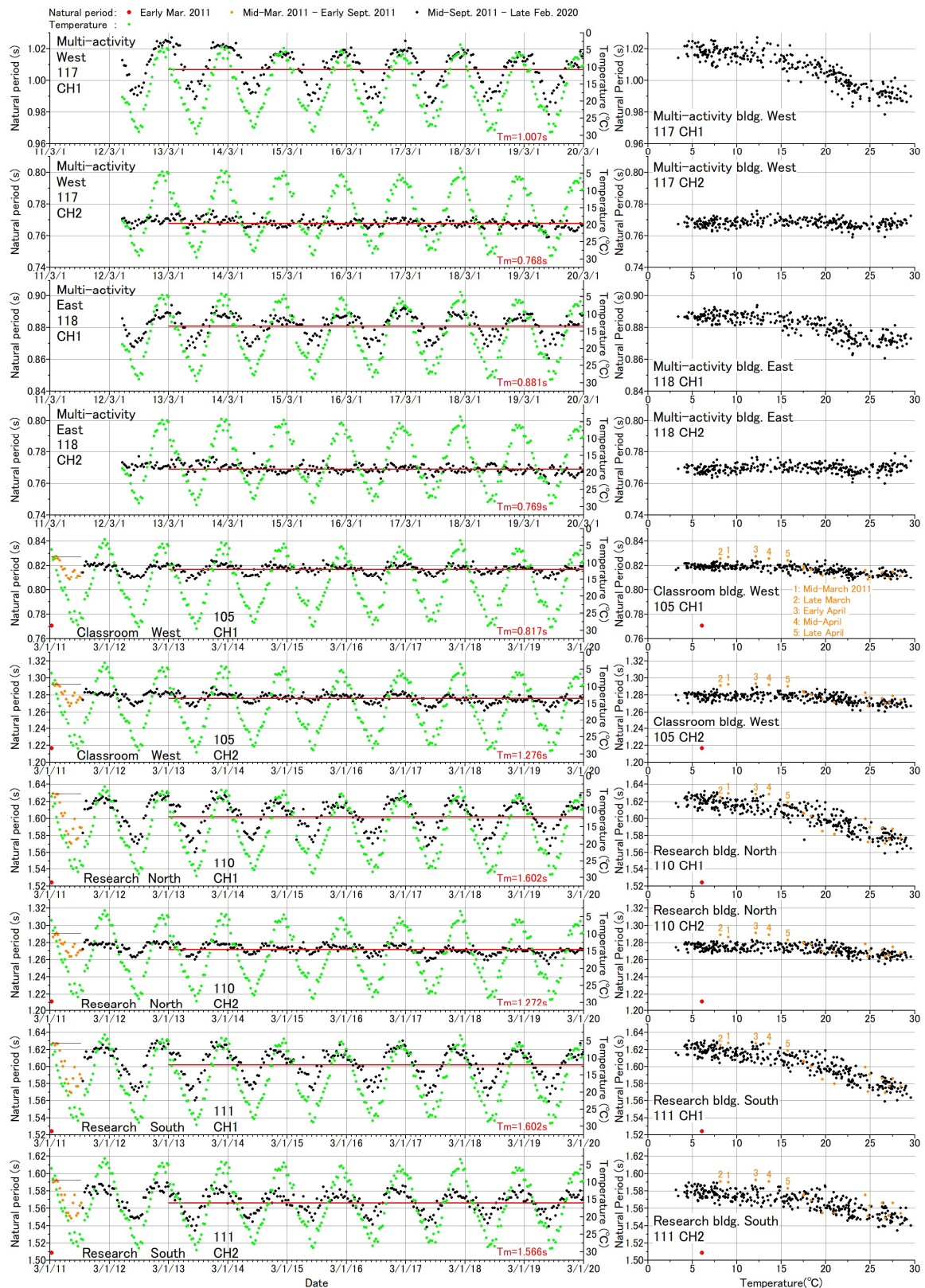


Fig. 3 Changes over time of the 10-day average of the natural periods estimated from the microtremors and the 10-day average of temperature (left) and the relationship between the 10-day averages of the natural periods and temperature (right). (The solid red line in each left figure shows the average of the 10-day averages of natural periods from early March 2013 to late February 2020. The value of “ T_m ” in the figure indicates the value on the y-axis of the red line.)

Table 3 Average value of the natural period (s) estimated from the microtremors in the first 10 days of March from 2011 to 2019

Installation position	Classroom bldg. West side/ top flr.		Research bldg. North side/ top flr.		Research bldg. South side/ top flr.	
	105		110		111	
Seismometer No.	105		110		111	
Direction	CH1	CH2	CH1	CH2	CH1	CH2
March 1–10, 2011	0.771	1.217	1.524	1.211	1.524	1.509
March 1–10, 2012	0.816	1.278	1.613	1.273	1.613	1.575
March 1–10, 2013	0.820	1.281	1.616	1.274	1.616	1.574
March 1–10, 2014	0.820	1.281	1.617	1.278	1.617	1.577
March 1–10, 2015	0.818	1.279	1.609	1.275	1.609	1.569
March 1–10, 2016	0.817	1.278	1.609	1.272	1.608	1.571
March 1–10, 2017	0.820	1.278	1.619	1.271	1.616	1.574
March 1–10, 2018	0.820	1.277	1.616	1.272	1.616	1.574
March 1–10, 2019	0.818	1.274	1.614	1.270	1.611	1.568
Avg. (2012–2019)	0.819	1.278	1.614	1.273	1.613	1.573
SD (2012–2019)	0.002	0.002	0.003	0.003	0.003	0.003
Difference* (s)	0.048	0.062	0.090	0.062	0.089	0.064
Rate of change** (%)	6.2	5.1	5.9	5.1	5.8	4.2

*: Difference between the average natural period in the first 10 days of March from 2011 to 2019 and the average natural period in the first 10 days of March 2011.

**: Rate of change = Difference* / Average natural period in the first 10 days of March 2011.

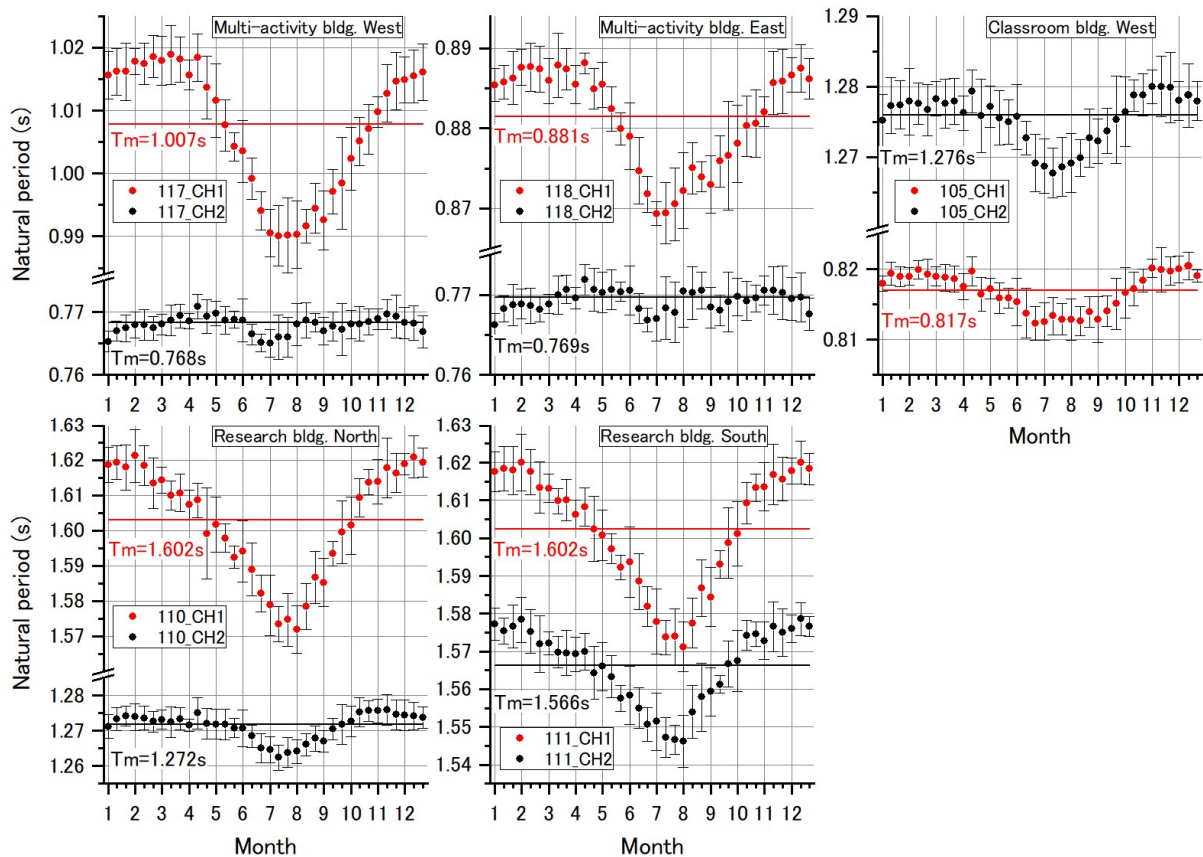


Fig. 4 Average and standard deviation of the 10-day averages of the natural periods estimated from the microtremors for the same 10-day period from March 2013 to February 2020

Table 4 Average and standard deviation (SD) of the 10-day averages of the natural periods estimated from the microtremors for the same 10-day period from March 2013 to February 2020

Mo.	Day	Installation Position		Multi-activity bldg.						Classroom bldg.				Research bldg.									
		Seismometer No.		West side/ top flr.			East side/ top flr.			West side/ top flr.				North side/ top flr.			South side/ top flr.						
		Direction		117		118		105				110			111								
		Avg. (°C)	SD (°C)	Avg. (s)	SD (s)	Avg. (s)	SD (s)	Avg. (s)	SD (s)	Avg. (s)	SD (s)	Avg. (s)	SD (s)	Avg. (s)	SD (s)	Avg. (s)	SD (s)	Avg. (s)	SD (s)				
1	1-10	6.76	0.99	1.016	0.004	0.765	0.002	0.885	0.002	0.766	0.001	0.818	0.001	1.275	0.004	1.619	0.005	1.271	0.003	1.618	0.005	1.577	0.004
	11-20	5.93	1.03	1.016	0.004	0.767	0.002	0.886	0.002	0.768	0.002	0.819	0.002	1.277	0.004	1.619	0.005	1.273	0.003	1.618	0.006	1.575	0.003
	21-EOM	6.03	1.45	1.016	0.005	0.767	0.002	0.886	0.003	0.769	0.003	0.819	0.001	1.277	0.003	1.618	0.006	1.274	0.003	1.618	0.006	1.577	0.006
2	1-10	5.60	0.97	1.018	0.002	0.768	0.002	0.888	0.002	0.769	0.002	0.819	0.001	1.278	0.005	1.621	0.008	1.274	0.004	1.620	0.008	1.578	0.006
	11-20	7.01	1.85	1.017	0.003	0.768	0.002	0.888	0.003	0.769	0.002	0.820	0.001	1.278	0.003	1.618	0.006	1.274	0.003	1.617	0.006	1.575	0.006
	21-EOM	7.94	1.20	1.019	0.003	0.767	0.002	0.887	0.003	0.768	0.002	0.819	0.002	1.277	0.004	1.613	0.007	1.273	0.003	1.613	0.007	1.572	0.007
3	1-10	8.78	1.61	1.018	0.004	0.768	0.002	0.886	0.003	0.769	0.001	0.819	0.001	1.278	0.002	1.614	0.004	1.273	0.003	1.613	0.004	1.572	0.003
	11-20	10.48	1.16	1.019	0.005	0.769	0.002	0.888	0.004	0.770	0.002	0.819	0.002	1.278	0.003	1.610	0.004	1.272	0.004	1.610	0.003	1.570	0.004
	21-EOM	11.26	1.44	1.018	0.004	0.769	0.002	0.887	0.003	0.771	0.002	0.819	0.002	1.278	0.003	1.611	0.005	1.273	0.003	1.610	0.005	1.570	0.006
4	1-10	12.91	1.82	1.016	0.002	0.769	0.001	0.885	0.002	0.770	0.001	0.818	0.002	1.276	0.002	1.607	0.004	1.272	0.002	1.606	0.004	1.569	0.005
	11-20	14.66	0.97	1.018	0.004	0.771	0.002	0.888	0.001	0.772	0.002	0.820	0.002	1.279	0.003	1.609	0.005	1.275	0.004	1.608	0.005	1.570	0.005
	21-EOM	16.47	1.39	1.014	0.005	0.769	0.003	0.885	0.003	0.771	0.003	0.816	0.002	1.276	0.005	1.599	0.013	1.272	0.004	1.602	0.009	1.564	0.007
5	1-10	18.04	1.16	1.012	0.006	0.770	0.002	0.885	0.003	0.770	0.003	0.817	0.001	1.277	0.003	1.602	0.008	1.272	0.004	1.601	0.007	1.566	0.006
	11-20	19.51	0.51	1.008	0.004	0.769	0.002	0.882	0.003	0.771	0.003	0.816	0.002	1.276	0.004	1.598	0.004	1.272	0.004	1.597	0.004	1.563	0.006
	21-EOM	21.03	0.54	1.004	0.002	0.769	0.001	0.880	0.002	0.770	0.001	0.816	0.001	1.275	0.003	1.592	0.003	1.271	0.003	1.592	0.003	1.568	0.003
6	1-10	21.46	0.59	1.004	0.005	0.769	0.003	0.879	0.004	0.771	0.003	0.815	0.003	1.276	0.005	1.594	0.009	1.271	0.005	1.594	0.009	1.558	0.008
	11-20	21.85	1.10	0.999	0.003	0.766	0.002	0.875	0.004	0.768	0.002	0.814	0.004	1.273	0.002	1.589	0.007	1.268	0.003	1.589	0.007	1.555	0.005
	21-EOM	23.01	0.52	0.994	0.003	0.765	0.001	0.872	0.002	0.767	0.001	0.812	0.002	1.269	0.004	1.582	0.005	1.265	0.004	1.582	0.005	1.551	0.005
7	1-10	24.15	1.92	0.991	0.004	0.765	0.002	0.869	0.002	0.767	0.003	0.813	0.003	1.269	0.004	1.579	0.009	1.265	0.004	1.578	0.009	1.551	0.008
	11-20	26.23	1.70	0.990	0.005	0.766	0.004	0.869	0.004	0.768	0.003	0.813	0.003	1.268	0.004	1.573	0.005	1.262	0.004	1.574	0.005	1.547	0.005
	21-EOM	26.90	1.29	0.990	0.006	0.766	0.003	0.871	0.005	0.768	0.004	0.813	0.002	1.269	0.004	1.575	0.007	1.264	0.004	1.574	0.007	1.547	0.004
8	1-10	28.11	0.76	0.990	0.005	0.768	0.003	0.872	0.005	0.770	0.005	0.813	0.003	1.269	0.004	1.572	0.007	1.264	0.003	1.571	0.007	1.546	0.007
	11-20	27.35	1.55	0.992	0.003	0.769	0.003	0.875	0.003	0.770	0.003	0.813	0.002	1.270	0.003	1.578	0.006	1.266	0.003	1.577	0.007	1.554	0.007
	21-EOM	26.29	1.74	0.994	0.004	0.768	0.001	0.874	0.002	0.771	0.002	0.814	0.002	1.273	0.004	1.587	0.007	1.268	0.004	1.587	0.007	1.558	0.009
9	1-10	25.33	1.95	0.993	0.005	0.767	0.002	0.873	0.004	0.768	0.003	0.813	0.003	1.272	0.003	1.585	0.007	1.267	0.003	1.584	0.008	1.559	0.006
	11-20	23.43	1.04	0.997	0.004	0.768	0.002	0.876	0.003	0.768	0.002	0.814	0.002	1.274	0.003	1.593	0.003	1.270	0.003	1.593	0.004	1.561	0.002
	21-EOM	22.24	1.05	0.998	0.007	0.767	0.004	0.877	0.007	0.769	0.004	0.815	0.004	1.275	0.006	1.600	0.009	1.272	0.006	1.599	0.009	1.567	0.006
10	1-10	21.56	1.22	1.002	0.005	0.768	0.002	0.878	0.005	0.770	0.002	0.817	0.004	1.276	0.005	1.601	0.008	1.273	0.004	1.601	0.009	1.568	0.008
	11-20	18.39	1.21	1.005	0.004	0.768	0.003	0.880	0.004	0.769	0.002	0.817	0.002	1.279	0.002	1.609	0.005	1.275	0.004	1.609	0.005	1.574	0.004
	21-EOM	16.83	0.75	1.007	0.004	0.768	0.002	0.881	0.004	0.770	0.002	0.818	0.002	1.279	0.003	1.614	0.004	1.276	0.003	1.613	0.004	1.575	0.003
11	1-10	15.42	1.33	1.010	0.002	0.769	0.002	0.882	0.002	0.771	0.002	0.820	0.001	1.280	0.002	1.614	0.006	1.276	0.003	1.614	0.006	1.573	0.005
	11-20	13.34	1.46	1.013	0.005	0.770	0.002	0.886	0.004	0.771	0.003	0.820	0.003	1.280	0.004	1.618	0.008	1.276	0.004	1.617	0.008	1.577	0.007
	21-EOM	11.35	1.06	1.015	0.005	0.769	0.003	0.886	0.004	0.770	0.003	0.820	0.002	1.280	0.005	1.616	0.006	1.275	0.004	1.616	0.006	1.575	0.006
12	1-10	9.79	1.23	1.015	0.004	0.768	0.003	0.887	0.002	0.769	0.003	0.820	0.002	1.278	0.003	1.619	0.003	1.274	0.004	1.618	0.003	1.576	0.004
	11-20	8.23	1.58	1.015	0.004	0.768	0.003	0.887	0.003	0.770	0.003	0.820	0.002	1.279	0.004	1.621	0.006	1.274	0.004	1.620	0.006	1.579	0.004
	21-EOM	7.46	1.00	1.016	0.005	0.767	0.003	0.886	0.003	0.768	0.002	0.819	0.001	1.278	0.003	1.619	0.004	1.274	0.003	1.618	0.004	1.577	0.003
Average		16.42	1.23	1.007	0.004	0.768	0.002	0.881	0.003	0.769	0.002	0.817	0.002	1.276	0.004	1.602	0.006	1.272	0.004	1.602	0.006	1.566	0.005
Maximum		28.11	1.95	1.019	0.007	0.771	0.004	0.888	0.007	0.772	0.005	0.820	0.004	1.280	0.006	1.621	0.013	1.276	0.006	1.620	0.009	1.579	0.009
Minimum		5.60	0.51	0.990	0.002	0.765	0.001	0.869	0.001	0.766	0.001	0.812	0.001	1.268	0.002	1.572	0.003	1.262	0.002	1.571	0.003	1.546	0.002
Range of variation*		22.51	-	0.029	-	0.006	-	0.019	-	0.006	-	0.008	-	0.012	-	0.049	-	0.013	-	0.049	-	0.032	-
Rate of range**		-	-	2.9	-	0.8	-	2.1	-	0.7	-	1.0	-	1.0	-	3.1	-	1.1	-	3.0	-	2.1	-

*: Range of variation means the difference between the maximum and minimum values.

** : Rate of range = Range of variation*/ Average of natural period from March 2011 to February 2020. Cells with a rate of range of 2% or more are shaded.

natural period remains almost constant when the outside air temperature falls below the temperature range described above has not been explained, but the phenomenon is thought to imply that there is a lower limit to the decrease in stiffness. This mechanism will be clarified in the future.

For the classroom and research buildings, natural periods were obtained in early March, just before the Tohoku Earthquake, and these are indicated by the red circles in Fig. 3. The graphs on the left side of Fig. 3 show that the natural periods increased after the Tohoku Earthquake and did not return to the natural period before the Tohoku Earthquake. Table 3 presents the natural periods in early March 2011–2019. The natural period at the beginning of March 2011 and the average of the natural period at the beginning of March in each year from 2012 to 2019 show an increase in period of 0.048–0.090 s, indicating an increase in the period of approximately 5% in terms of the rate of change.

During the Tohoku Earthquake, cracks were observed in partition walls and exterior materials, which are nonstructural members, at several locations in the buildings. Nonstructural members are not evaluated as stiffnesses even at the design stage but are in fact considered to contribute to the stiffness of the entire building. Therefore, the damage to the nonstructural members may have caused a slight reduction in stiffness, resulting in an elongation of the natural period.

A temporary elongation of the natural period can also be observed in addition to this constant natural period elongation. Each graph on the left side of Fig. 3 shows a horizontal line passing through the maximum natural period from early March 2011 to early September of the same year, which is larger than the average value of the natural period since then. Therefore, the natural periods for the 6-month period from mid-March to early September, immediately after the Tohoku Earthquake, are shown in orange. As shown in the graphs on the right side of Fig. 3, the natural period tended to be longer for approximately 2 months until late April. This may be because the stiffness has recovered slightly due to the solidification of cracks, although the stiffness has not returned to the level before the Tohoku Earthquake.

The natural period varies seasonally; therefore, current natural period must be compared with that of the same period in previous years to determine the condition of the structure. Figure 4 and Table 4 show and present the obtained average and standard deviation of the 10-day averages of the natural periods estimated from the microtremors for the same 10-day period from March 2013 to February 2020. It is important to continuously monitor the natural period and accumulate knowledge on building maintenance and management through comparison and discussion with the present record. Therefore, although Fig. 4 and Table 4 provide almost the same information, specific numerical values are also presented in Table 4 to facilitate the quantitative implementation of this comparison and study in the future. Figure 4 shows the average \pm standard deviation with error bars and shows that the natural period varies seasonally, with a different range of range of variation. In the CH1 direction on the west and east sides of the multi-activity building, the CH1 direction on the north side of the research building, and the CH1 and CH2 directions on the south side of the research building, the error bars for the winter and summer are far apart, indicating that the natural periods are significantly different between the winter and summer. Table 4 presents the rate of variation of the natural period. The rate of variation in these locations is 2%–3%, which is larger than that of the other locations, which is approximately 1%. The reason why the rate of change tends to be large in the CH1 direction is assumed to be because the temperature gradient in the columns increases in the CH1 direction due to the relationship between the building orientation and sunlight and that stiffness changes⁵⁾ tend to occur in the CH1 direction.

5. EVALUATION OF THE AMPLITUDE-DEPENDENT CHARACTERISTICS OF THE VIBRATION PROPERTIES USING SEISMIC RECORDS

Section 4 examined the variation of natural period at the microtremors level. This section estimates the natural period and damping ratio using seismic records. The ARX model^{15), 16)} has been widely used for mode identification methods and is not newly developed in this study. However, as mentioned in Section 1, this article is also intended to serve as a resource, and a brief description of the estimation method is given below.

5.1 Method for estimating the natural period and the damping ratio

The ARX model is used to estimate the natural period and damping ratio. The ARX model is given by the following equation:

$$y(t) + a_1y(t-1) + \dots + a_{n_a}y(t-n_a) = b_1u(t-n_k) + b_2u(t-1-n_k) + \dots + b_{n_b}u(t-n_b+1-n_k) + e(t) \quad (1)$$

where $y(t)$ and $u(t)$ are the output and input at time t , respectively, a_n and b_n are the model coefficients

for the output and input, respectively, n_a and n_b are the model orders of the output and input, respectively, n_k is the delay time, and $e(t)$ is the white noise with zero mean value. Equation (1) can be expressed using the time-shift operator q as

$$A(q)y(t) = B(q)u(t) + e(t) \quad (2)$$

where $A(q)$ and $B(q)$ are polynomial functions defined as follows:

$$A(q) = (1 + a_1q^{-1} + a_2q^{-2} + \dots + a_{n_a}q^{-n_a}) = 1 + \sum_{j=1}^{n_a} a_j q^{-j} \quad (3)$$

$$B(q) = b_1q^{-n_k} + b_2q^{-1-n_k} + \dots + b_{n_b}q^{-n_b+1-n_k} = \sum_{j=1}^{n_b} b_j q^{-j+1-n_k} \quad (4)$$

The model coefficients are identified by applying the least-squares method to minimize the sum of squares of $e(t)$ in Eq. (2), using $y(t)$ and $u(t)$, the model orders n_a and n_b , and the delay time n_k set in advance in the time window. Let the time-shift operator q be the variable z in the z -transform. The transfer function $H(z)$ of the system determined by the identified ARX model is expressed in the z -transform as follows:

$$H(z) = \frac{B(z)}{A(z)} \quad (5)$$

On the contrary, from the correspondence with the transfer function of the system in the multi-degree-of-freedom model, the natural period T_j and damping ratio h_j of the j -th-order mode can be obtained from the following equations:

$$T_j = \frac{2\pi\Delta t}{\left| \log_z p_j \right|} \quad (6)$$

$$h_j = \frac{-T_j \log \left| z p_j \right|}{2\pi\Delta t} \quad (7)$$

where $z p_j$ is the pole with $A(z) = 0$ and Δt is the sampling period of the seismic record. From the above, the natural period and damping ratio can be estimated from the input and output seismic records by setting the model orders n_a , n_b , and n_k . These identifiers depend on the model order; thus, it is necessary to set the model order appropriately. Section 5.3 describes the specific method for determining the model order. The seismic records used in the analysis are then described.

5.2 Seismic records used for the analysis

Estimating the natural period requires seismic records that correspond to the input and output. Since the seismic isolation system is a nonlinear system with amplitude dependence, the input side was divided into the upper and lower seismic isolation layer, and the output side was the top floor of each building to estimate the natural period. The pairs of seismometers were selected to be as vertically aligned as possible, as presented in Table 5.

The seismic records used are the records of 181 earthquakes out of 196 earthquakes obtained between November 1, 2010, and February 29, 2020, in the list of seismic records published on the web by the authors¹⁷⁾, excluding those with very small amplitudes or with problems in the time synchronization of the network accelerometers.

Considering seismograph 101 as representative of the input side, Fig. 5 shows the relationship between the JMA seismic intensity and the JMA magnitudes¹⁸⁾ of the 181 earthquakes used in the

Table 5 Input side and output side seismometers and model order n_a when using the ARX model

Installation position	Multi-activity bldg.				Classroom bldg.		Research bldg.				
	West side		East side		West side		North side		South side		
Period*	-3/10	3/11-	-3/10	3/11-	-3/10	3/11-	-3/10	3/11-	-3/10	3/11-	
Number of earthquakes	0	96	0	96	7	174	7	174	7	174	
Seismometer No. ** (output/input)	117/006		118/010		105/007		110/008		111/012		
Model order n_a	CH1	-	90	-	80	70	100	130	180	160	220
	CH2	-	50	-	40	190	200	140	200	180	210
Seismometer No. ** (output/input)	117/001		118/002		105/003		110/101		111/005		
Model order n_a	CH1	-	130	-	70	80	90	140	180	110	210
	CH2	-	50	-	50	170	190	130	200	170	200

*: “-3/10” represents the period from 11/1/2010 to 3/10/2011, and “3/11-” represents the period from 3/11/2011 to 2/29/2020.

**: Seismometers used in the analysis are marked with blue boxes in Fig. 1.

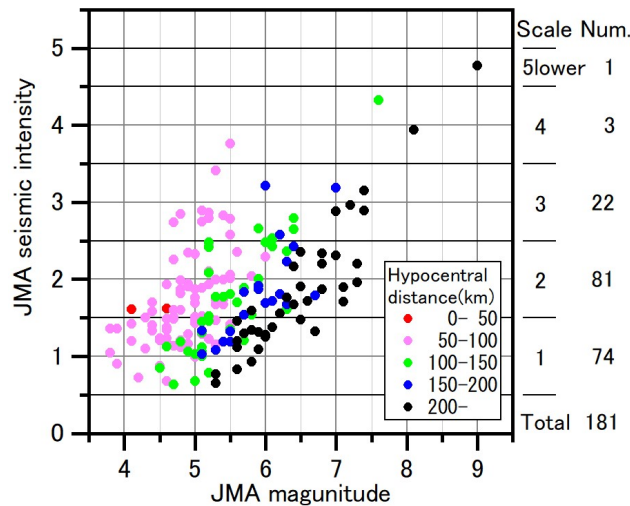


Fig. 5 Relationship between the JMA magnitudes¹⁸⁾ of the 181 earthquakes used in the analysis and the measured JMA seismic intensities at seismograph 101

analysis. The range of the JMA seismic intensity scale on the input side was generally in the range of “1” to “5 lower.”

Figure 6 shows the relationship between the maximum acceleration on the input and output sides, as presented in Table 5, to examine the characteristics of the seismic records used in the analysis. For the classroom and research buildings, the results before, during, and after the Tohoku Earthquake are shown in different colors. Since there is little difference in the trends before and after the Tohoku Earthquake, regression equations, excluding only the results of the Tohoku Earthquake, were obtained and are shown by the solid lines in each graph. The dashed lines represent the extrapolations up to the results of the Tohoku Earthquake. The coefficient of determination (R^2) for each building ranged from 0.87 to 0.96, indicating a good fit of the regression equation. However, if the change in the natural period due to the amplitude dependence in reference 10 and later is interpreted as a decrease in the stiffness of the structure, the response relationship in Fig. 6 should change before and after the Tohoku Earthquake, and a downward rightward trend should also be apparent. Therefore, it is difficult to interpret the linearity of the response relationship seen in the figure. The change in the natural period mainly reflects the effect of the nonstructural and seismic isolation members, whereas the linear response relationship in Fig. 6 is believed to reflect the effect of the structural members. Therefore, Fig. 6 can indicate that the structural members were not damaged.

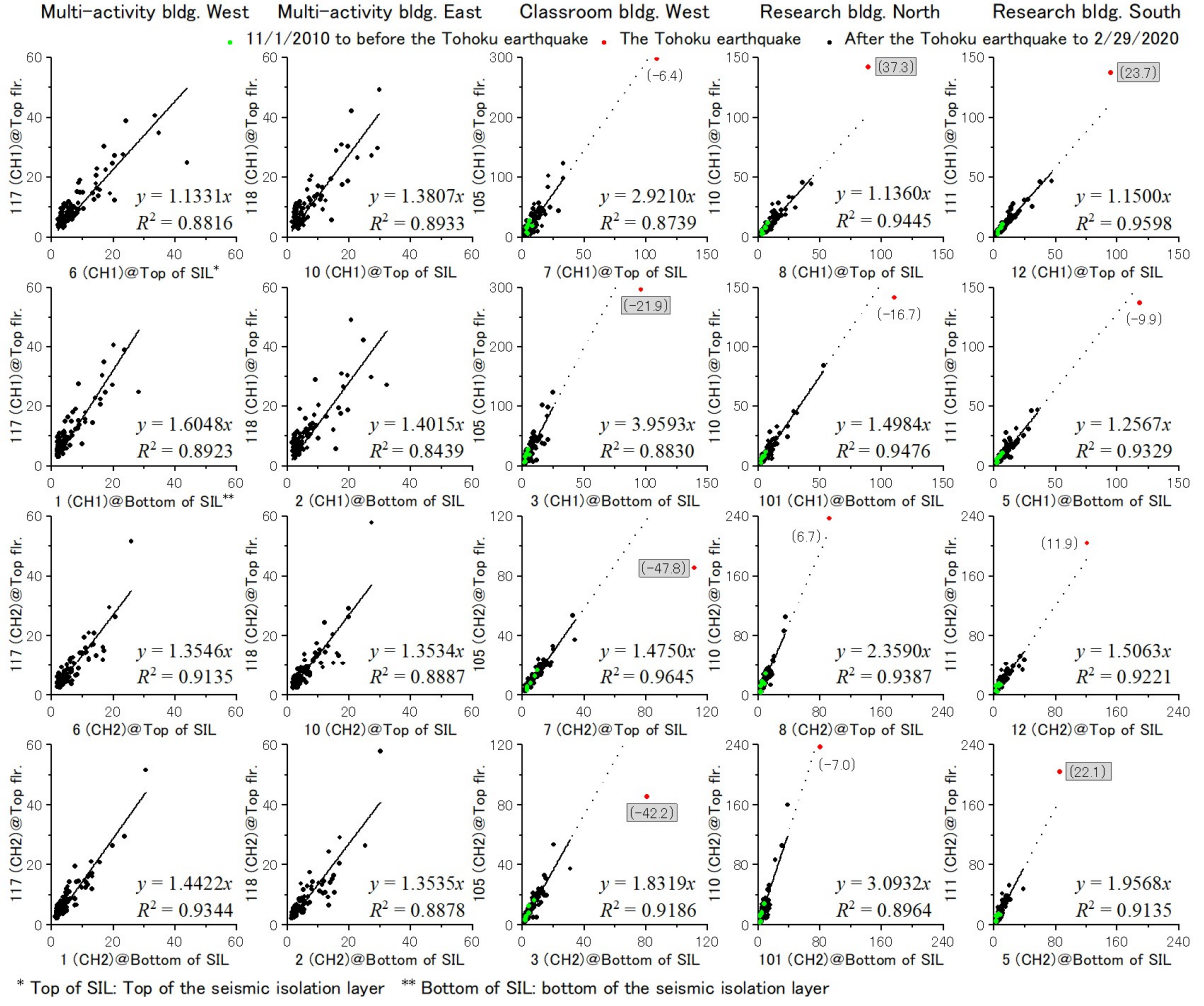


Fig. 6 Relationship between the maximum acceleration on the input and output sides, as presented in Table 5. (Regression equations, excluding only the results of the Tohoku Earthquake, were obtained and are shown by the solid lines in each figure. The dashed lines indicate the extrapolations up to the results of the Tohoku Earthquake. Each figure also shows the value of the outlier index defined in Eq. (8). If the absolute value of the outlier index is $>20\%$, it is significantly considered to be an outlier, and the number is shaded.)

Next, the plots of the response relationship for the Tohoku Earthquake are discussed. The dashed lines indicate the extrapolated intervals of the regression equation, and it can be seen that the plots for the Tohoku Earthquake are sometimes near the dashed lines and sometimes far off. Therefore, the outlier index is defined as an indicator of the degree of outlier as follows:

$$\text{outlier index (\%)} = \frac{\text{Maximum acceleration at the top floor} - \text{Predicted value}}{\text{Predicted value}} \times 100 \quad (8)$$

where the predicted values are obtained by substituting the maximum acceleration of the seismometers located above or below the seismic isolation layer into the regression equation. The figures also show the value of the outlier indices. If the absolute value of the outlier index is $>20\%$, it is significantly considered to be an outlier, and the number is shaded.

First, the outlier index obtained using seismic records for the bottom of the seismic isolation layer and top floor is discussed. This outlier index is considered to correspond to the seismic isolation effect. The outlier index is significantly negative in two directions on the west side of the classroom building,

and it is also negative in two directions on the north side of the research building and CH1 direction on the south side, ranging from -7.0% to -16.7% , indicating that there is some seismic isolation effect. However, in the CH2 direction on the south side of the research building, the outlier index is larger in the positive direction, indicating no seismic isolation effect.

Next, the outlier index obtained using seismic records for the top of the seismic isolation layer and top floor is discussed. This outlier index is considered to correspond to the seismic isolation effect. In the CH1 direction on the north and south sides of the research building, the outlier index is very large in the positive direction, and in the CH2 direction, they are also relatively large in the positive direction, indicating that the superstructure of the research building was amplified compared to other earthquakes. However, on the west side of the classroom building, the outlier index in the CH2 direction shows large negative values, and the outlier index in the CH1 direction also shows negative values, indicating that the superstructure was damped compared to other earthquakes. As can be seen in Photo 1 and Fig. 1(a), the research building has a piloti structure, making it a top-heavy structure. Moreover, it is thought that the Tohoku Earthquake, which had a long duration, caused relatively large shaking compared to other earthquakes. Conversely, nonlinearity of the structural members could be a possible reason for the damping of the classroom building. However, since the average inter-story drift angle¹³⁾ obtained from the acceleration records has a maximum of $1/241$ rad in the CH1 direction between seismometers 007 (B1) and 102 (fourth floor) on the west side of the classroom building, it is difficult to consider that nonlinearity is a reason. Another reason is that the amplitude of the classroom building was suppressed by the L-shaped connection of the research and classroom buildings. Therefore, it can be inferred that the increase or decrease in the response value of the superstructure is due to the irregularity of the superstructure.

5.3 Relationship seismic intensity index and natural period of the superstructure with and without seismic isolation layer

The ARX model is used to estimate the natural period of the superstructure with and without the seismic isolation layer. The seismic record of the top floor is used as the output, and the seismic records below and above the seismic isolation layer are used as the input. As mentioned above, an optimal model order must be determined when using the ARX model. The next section describes the method used to determine the model order in this study.

5.3.1 Method of determining the model order

The model order n_b was assumed to be $n_b = n_a + 1$ based on reference 11, and the delay time n_k was determined to be $n_k = 0$ based on the examination results of the impulse response function¹⁹⁾ using input–output waveforms. Therefore, n_a is the only parameter to be estimated. In this study, n_a was set between 10 and 250, in increments of 10, and the correlation coefficients between the identified natural periods and the seismic intensity indices were obtained for each n_a . The model order was set to n_a when the correlation coefficient was the largest. On the other hand, as seismic intensity indices, the maximum acceleration, maximum velocity, spectral intensity (SI), and JMA seismic intensity, calculated with one component on the output and input sides, were considered. The Tohoku Earthquake is expected to have caused a change in the response system of the buildings. However, only seven seismic records are found prior to the Tohoku Earthquake, and the analysis results of microtremors indicate that the response system may have been in transition for some time after the Tohoku Earthquake. Therefore, the seismic records used to determine the model order n_a are those observed between September 11, 2011, and February 29, 2020, when the response system is considered to have stabilized. Consequently, seismic records of 96 earthquakes in the multi-activity building and 116 earthquakes in the classroom and research buildings were used for the study. The time window used for identification was 41 s, 4 s before the arrival of the S-wave in the seismic waveform.

The correlation between the identified natural period and the seismic intensity index was stronger when the seismic intensity index on the output side (above or below the seismic isolation layer) was

used than on the input side (top floor). The correlation between various indices and the natural period was highest for SI (logarithmic value), roughly the same for maximum velocity (logarithmic value) and JMA seismic intensity, and lowest for maximum acceleration (logarithmic value). Yamamoto et al.²⁰⁾ reported a relatively high correlation of the natural frequencies obtained from the transfer function and the SI (logarithmic value) of the input side. They also obtained a regression equation for the natural frequencies for a 60 m-high steel construction with a relatively similar scale and structure type to that of the research building. The R^2 values calculated from the correlation coefficients in the same reference are 0.29 and 0.43 for the short side direction and for the long side direction, respectively, which are much smaller than the R^2 values obtained in the present study.

The regression analysis between the natural period and the SI of the top floor at each model order n_a was conducted using the following equation:

$$T_0 = a + b \log_{10}(\text{SI}) \quad (9)$$

where T_0 is the natural period (s) and a and b are the regression coefficients (s). Figure 7 shows the relationship between n_a , R^2 , and regression coefficients a and b . R^2 can have a sharp peak or a gradual peak. In this study, it is assumed that SI can explain the natural period, so the model order is determined by n_a when R^2 is at its maximum. In the same figure, a vertical line is drawn at the position of the model order n_a . It can be observed that the changes of regression coefficients a and b around the vertical line are small; hence, further refinement of n_a is not necessary in the present method of determining n_a . In some channels, R^2 drops rapidly to the right of the R^2 peak. For example, the plots of the analysis results for the CH2 direction for seismographs 105 and 007 (hereafter denoted as “105/007”) show that the R^2 value is maximum at $n_a = 200$, but is almost zero after $n_a = 210$. This is because the natural periods for some earthquakes were overestimated, resulting in outliers in the regression analysis and reducing the R^2 values. Outliers were not excluded from the regression analysis based on the idea that the occurrence of outliers reflects the influence of n_a . From the above, the determined model order n_a and R^2 values range from 40 to 220 and from 0.72 to 0.93, respectively. The relationship between the natural period of the structure and n_a is discussed here. The natural period estimated from the microtremors is used instead of the seismic motion. Figure 8 shows the relationship between the model order n_a and the natural periods indicated by the averages presented in Table 4. A rightward linear relationship is observed between natural period and n_a .

Next, for the classroom and research buildings, the determined model order was also applied to seismic records prior to September 11, 2011, and its validity was examined. As a result, in some cases, the identified natural periods and SIs did not show sufficient correlation before the Tohoku Earthquake. Therefore, the correlation between SI and the identified natural period for the seismic records before the Tohoku Earthquake was examined by setting n_a between 10 and 250 in increments of 10 again. Figure 9 shows the results, as in Fig. 7. The figure shows that the R^2 - n_a curve often has no clear peak or multiple peaks, making it difficult to determine the model order. Therefore, the model order before the Tohoku Earthquake was set to the position of the first maximum R^2 value in the range smaller than n_a determined above. In Fig. 9, a vertical line is drawn at the location of the model order n_a . As in Fig. 7, the changes of regression coefficients a and b around the vertical line are small; hence further refinement of n_a is not necessary in the current method of determining n_a . The reason why the model order n_a here is limited to a range shorter than n_a determined from seismic records after the Tohoku Earthquake is that the natural period is considered to have been shorter before the Tohoku Earthquake than it is now. This is because n_a becomes smaller as the natural period becomes shorter, as shown in Fig. 8. From the above, the determined model order n_a and R^2 values range from 70 to 190 and from 0.83 to 0.99, respectively. The reason for the larger R^2 value may be that there were only seven earthquakes used in the analysis.

Table 5 summarizes the determined model orders n_a . In this study, n_a is statistically determined by assuming a correlation between the natural period and the seismic intensity index. Therefore, applying the present method of determining the model order is difficult to structures with few seismic records or those that do not meet the above assumptions. The study of how to determine the model order is very

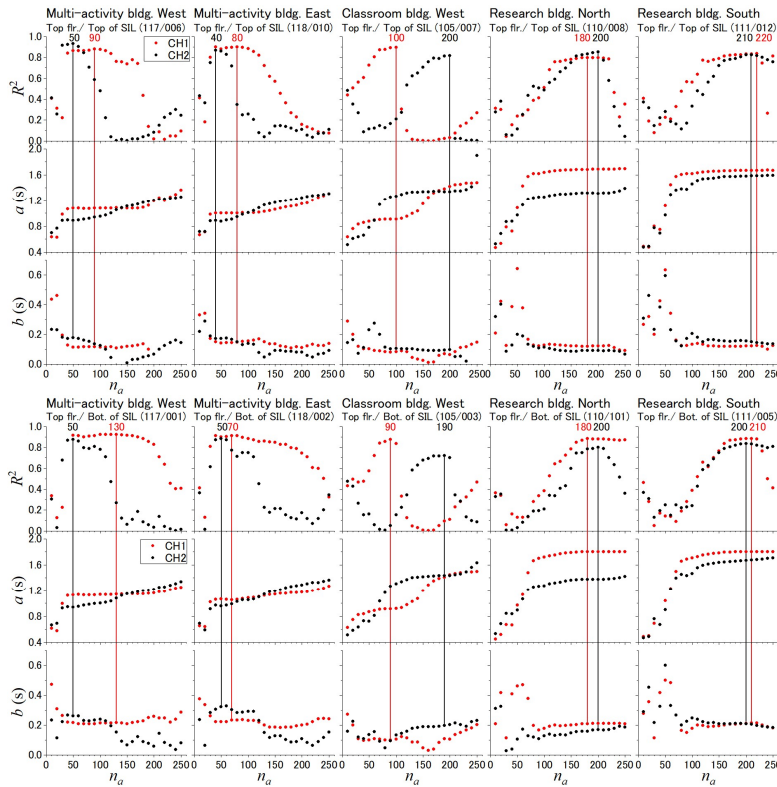


Fig. 7 Relationship between the model order n_a , the coefficient of determination R^2 , and the regression coefficients a and b for earthquake records from September 11, 2011, to February 29, 2020

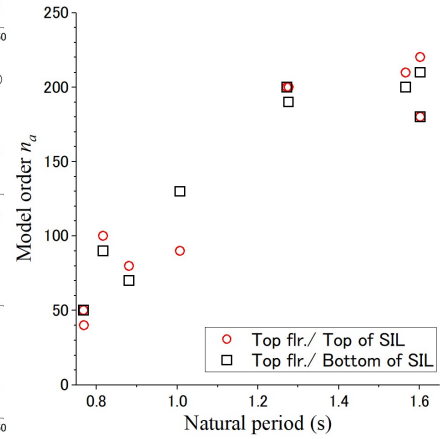


Fig. 8 Relationship between the model order n_a and the natural periods estimated from the microtremors

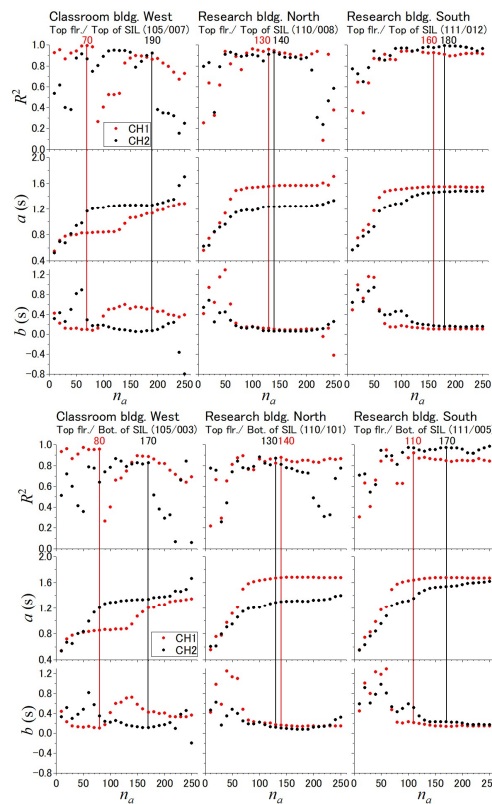


Fig. 9 Relationship between the model order n_a , the coefficient of determination R^2 , and the regression coefficients a and b for earthquake records before the Tohoku Earthquake

important. A future study plans to use the Akaike information criterion (AIC)¹⁶⁾, which is used to determine model fitness, aims to compare the simulated and observed waveforms¹⁶⁾ to investigate the relationship with the model order obtained in this study.

5.3.2 Relationship between the spectral intensity and the natural period of the superstructure with and without seismic isolation layer

Figure 10 shows the relationship between the natural period and the SI of the top floor. Figure 10 also shows the average of the natural periods of the microtremors from March 2013 to February 2020 presented in Table 4 as blue squares and the maximum and minimum values of the 10-day average of natural periods as error bars. The variation range of the natural period estimated from earthquake ground motion is larger than that estimated from the microtremors, and that it has a roughly linear relationship with the SI (logarithmic value). For the classroom and research buildings, the average natural period of the microtremors at the beginning of March 2011 is indicated by a green square, and the natural periods obtained from seismic records are divided into four periods: (1) before the Tohoku Earthquake, (2) during the Tohoku Earthquake, (3) from the Tohoku Earthquake to September 10, 2011, and (4) from September 11, 2011, to February 29, 2020. Circles with different colors indicate the results for each period. Periods (3) and (4) correspond to the transient and stable periods of the vibration characteristics after the Tohoku Earthquake. As described in Section 4, the natural period of the Tohoku Earthquake showed a temporary increase of approximately 2 months as well as a permanent increase. Therefore, September 10, 6 months after the earthquake, when this temporary increase was considered to have been fully resolved, was set as the boundary date for periods (3) and (4). However, Fig. 10 shows no clear difference between periods (3) and (4).

Solid green and black lines indicate the regression equations for periods (1) and (4), respectively, while dashed lines indicate the extrapolated intervals. The R^2 values range from 0.72 to 0.99, indicating that the regression equation fits well. As with the microtremors, the natural period estimated from the seismic motion is found to have increased after the Tohoku Earthquake. Since the natural period is amplitude dependent, substituting SI of 3.0 cm/s into the regression equations for periods (1) and (4) and examining the change in the natural period show that the natural period increased by approximately 6%–10%. Although this is slightly larger than the 4%–6% change in the natural period estimated from the microtremors presented in Table 3, it is considered to be an elongation of the period due to damage to nonstructural members caused by the Tohoku Earthquake described in Section 4. Based on the relationship between SI and the measured seismic intensity calculated with one component, the SI of 3.0 cm/s corresponded to a JMA seismic intensity of approximately 3.0.

On the other hand, for the Tohoku Earthquake, the natural periods between the top of the base isolation layer and the top floor and between the bottom of the base isolation layer and the top floor are consistent with the extrapolation of the regression equation for period (4). However, the natural period between the bottom of the base isolation layer and the topmost floor in the CH2 direction is significantly extended from the trend of the regression equation for period (4). The maximum inter-story drift in the seismic isolation layer of the classroom and research buildings was 4.5–5.2 cm in the CH1 direction, while the maximum inter-story drift in the CH2 direction was 6.6–9.5 cm, which is 1.3–1.8 times greater than in the CH1 direction⁹⁾. This may have caused a reduction in the stiffness of the seismic isolation layer, especially in the CH2 direction, resulting in a large elongation of the natural period.

The regression equation for the multi-activity building is also shown as a solid line in Fig. 10. For CH2 in the long side direction, the relationship between natural period and SI on the west and east sides tends to be almost the same. However, for CH1 in the short side direction, the natural period tends to be shorter on the east side. This may be due to the fact that the west side has a deeper foundation and substantially higher building height than the east side and has fewer columns and less rigidity due to the presence of a hall (see Fig. 1(b)).

The above results indicate a linear relationship between the natural period and SI (logarithmic value). If a different response trend from this regression equation is observed in the future, damage or alteration of the superstructure or seismic isolation members can be suspected.

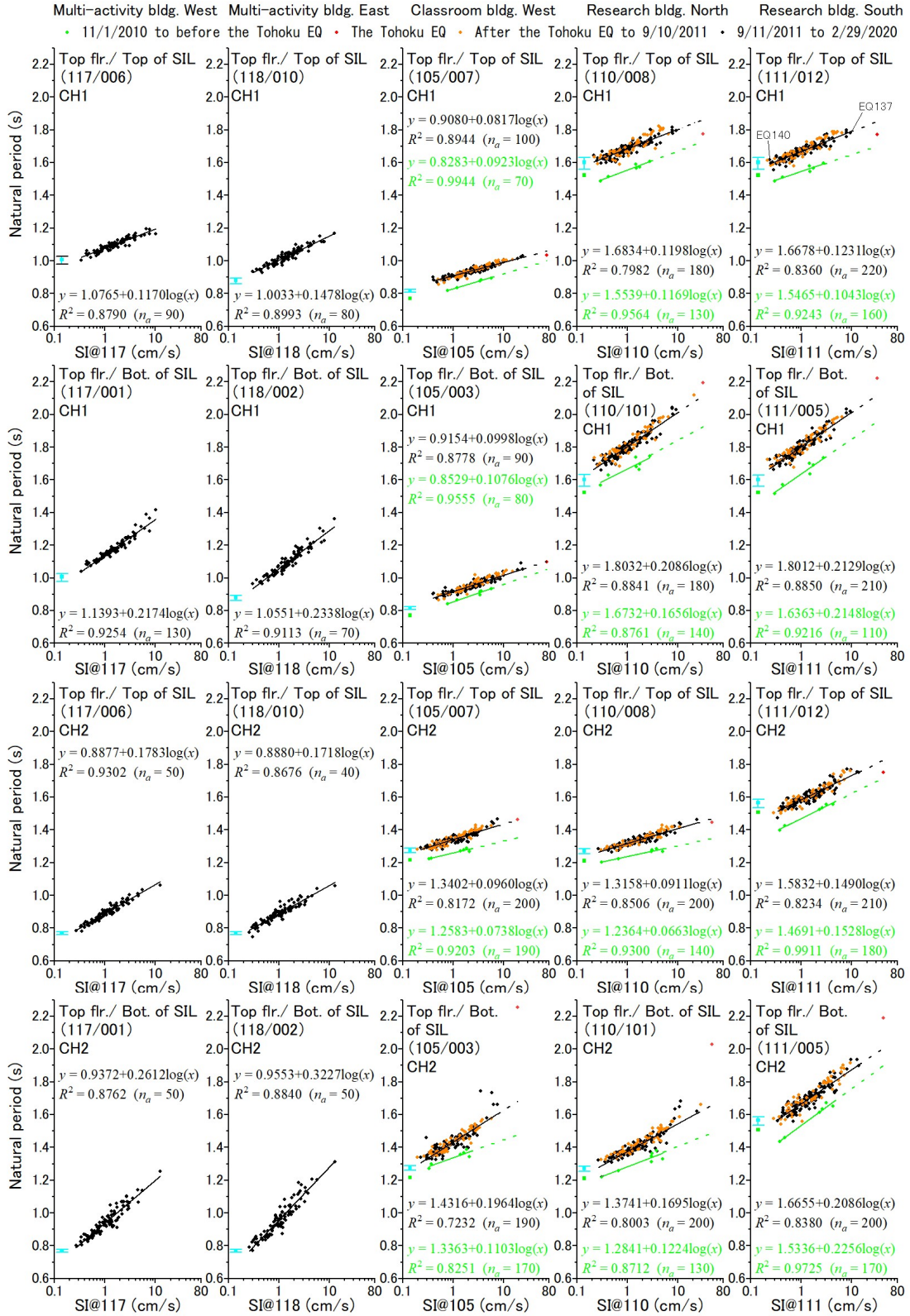


Fig. 10 Relationship between the natural period estimated from seismic records and the spectral intensity (SI) of the top floor (The green square with SI of 0.14 cm/s shows the average natural period estimated from microtremors in early March 2011, and the blue square and error bars show the average, maximum, and minimum of the 10-day averages of the natural periods estimated from the microtremors from March 2013 to February 2020.)

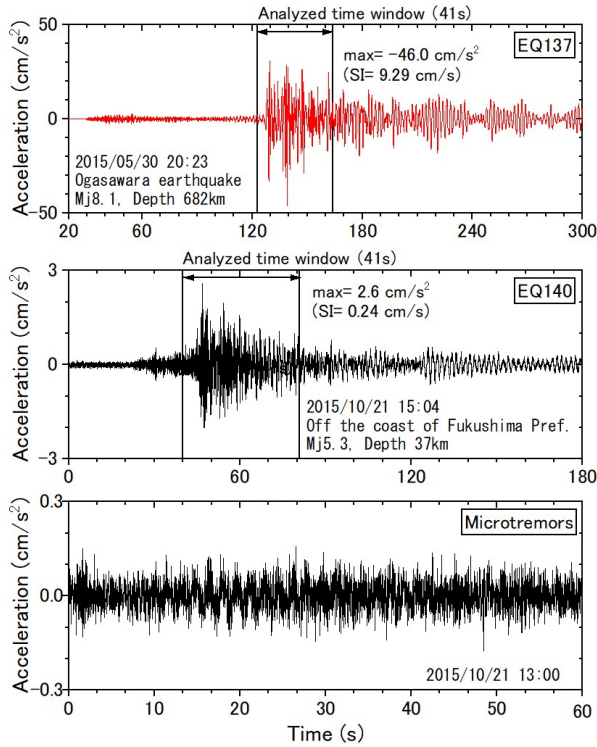


Fig. 11 Seismic records and a microtremor record at seismograph 111 on the top floor on the south side of the research building (CH1 direction)

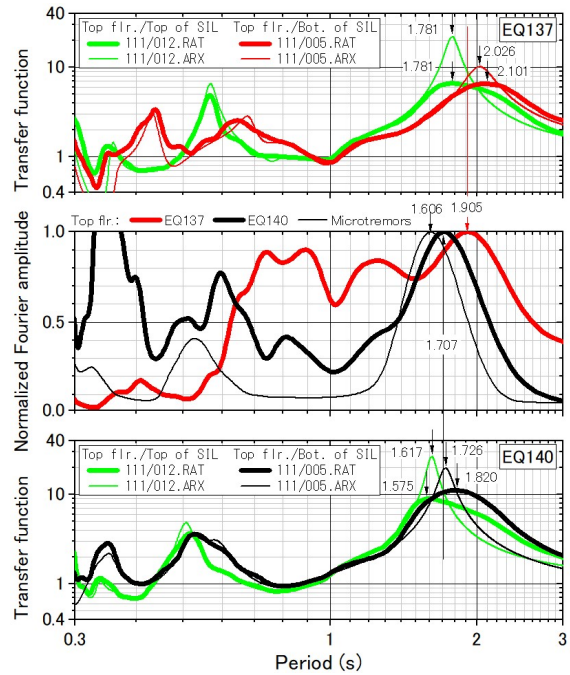


Fig. 12 Comparison of the normalized Fourier amplitudes (middle panel) of the seismic and microtremor records shown in Fig. 11 and the transfer functions of the seismic records EQ137 (top panel) and EQ140 (bottom panel) obtained from the ARX model and spectral ratio

5.4 Relationship between the natural period obtained from the microtremors and earthquake ground motions

Since the natural period obtained from the seismic record uses the transfer function between input and output, it is clear that it is the natural period of the system between these inputs and outputs. On the other hand, only the spectrum of the top floor is used for the microtremors, which may include the influence of the ground, as mentioned in Section 4, and it is unclear which system has the natural period. Therefore, this section discusses the relationship between the natural period obtained from the microtremors and seismic motions.

For the CH1 direction of seismograph 111, the seismic records of EQ137 and EQ140, with the maximum and minimum SI values in period (4), are treated as strong and weak tremors, respectively. Figure 11 shows these waveforms. The earthquake numbers correspond to those in reference 13. Figure 11 also shows a record of microtremors approximately 2 h before EQ140. The normalized Fourier amplitudes are shown as these spectra in the middle panel of Fig. 12. The FFT and a Parzen window with a bandwidth of 0.2 Hz were used to obtain the spectrum for the seismic record, with a cosine taper applied to the 10% at both ends of the time window and a trailing zero to increase resolution on the long-period band. The same procedure in Section 4 for the 10-min recording (only 1 min is shown in Fig. 11) is used to obtain the spectrum of the microtremor recording. Although each spectrum includes the effects of the ground and the earthquake source as well as the building, it can be seen that the larger the amplitude of the record, the longer the peak period.

The upper and lower panels of Fig. 12 show the transfer function obtained from the ARX model (ARX) and the transfer function obtained from the spectral ratio (RAT). The transfer functions are

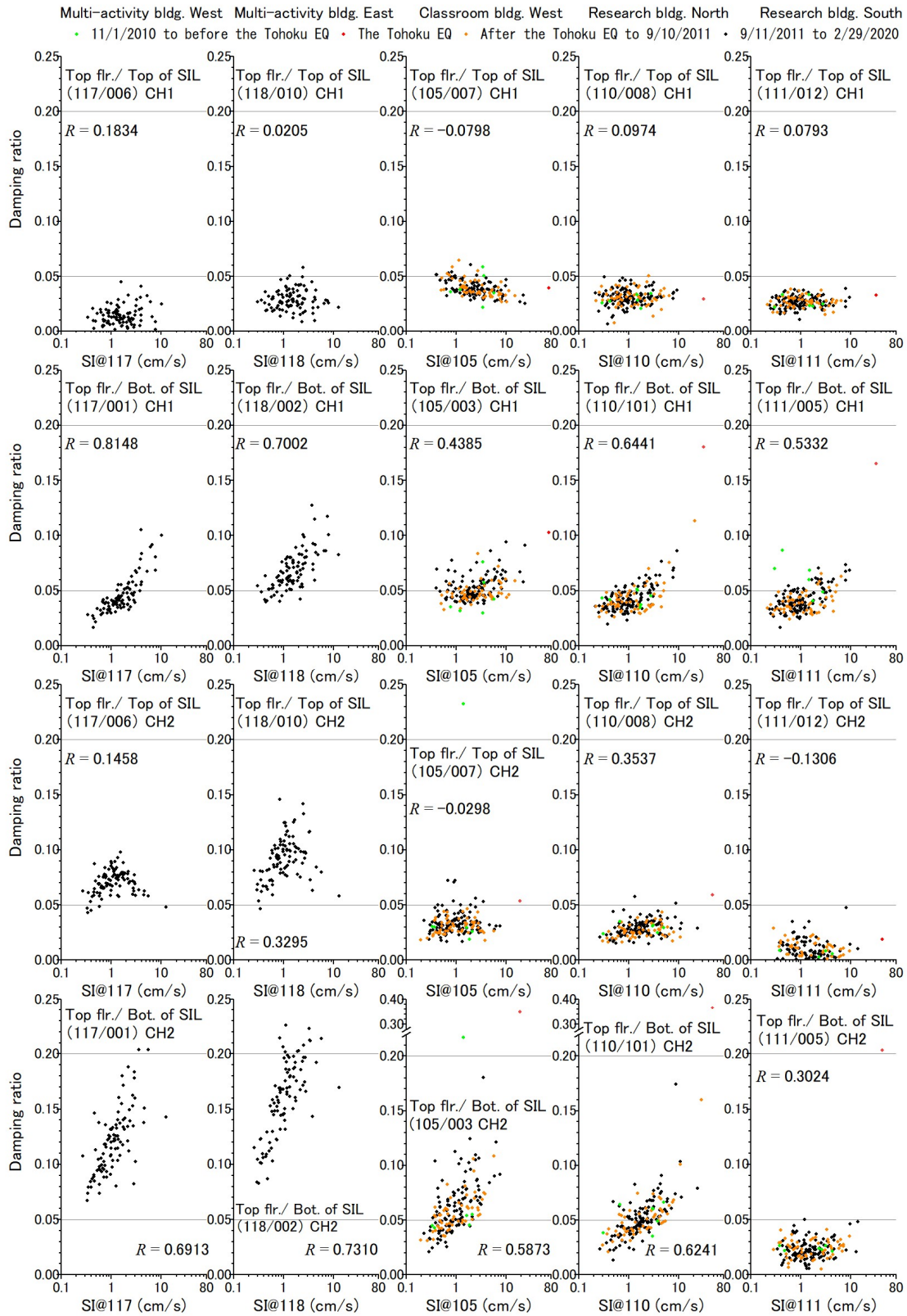


Fig. 13 Relationship between the damping ratio estimated from seismic records and the spectral intensity (SI) on the top floor

obtained between the top of the seismic isolation layer and the top floor (111/012) and between the bottom of the seismic isolation layer and the top floor (111/005). The two transfer functions are similar; however, the transfer function (ARX) shows a more distinct peak on the long-period band. This is believed to be due to the lower resolution of the long-period band of the spectrum with the FFT.

As can be seen from the middle and bottom panels of Fig. 12, the peak period (1.707 s) of the weak ground motion spectrum (EQ140) and the peak period (1.726 s) of the transfer function (ARX) between the bottom of the seismic isolation layer and the top floor are almost the same, suggesting that the weak ground motion spectrum can be regarded as a response with the bottom of the isolation layer as the fixed base. The peak period of the microtremor spectrum (1.606 s) is also close to the peak period of the weak ground motion, and the microtremor spectrum is also inferred to be the response with a fixed base below the seismic isolation layer. As can be seen from the middle and top panels of Fig. 12, the peak period (1.905 s) of the spectrum for the strong ground motion (EQ137) is between the peak period (2.026 s) of the transfer function (ARX) between the bottom and top floors of the base isolation layer and the peak period (1.781 s) between the top floors and top of the base isolation layer, indicating a different response from the weak ground motion.

The above results indicate that the natural period obtained from the microtremors corresponds to the natural period between the bottom and top floors of the seismic isolation layer during a weak earthquake and tends to be slightly shorter than that of the latter. As confirmed in Fig. 10, the natural periods estimated from the microtremors are consistent with this trend, except for CH2 at 111/005. On the other hand, the natural period estimated from the microtremors tends to be as long as or longer than the natural period between the top of the seismic isolation layer and the top floor during a weak earthquake. Therefore, the natural period obtained from the microtremors in this article is considered to be the natural period of the structure above the seismic isolation layer.

5.5 Relationship between the spectral intensity and the damping ratio of the superstructure with and without the seismic isolation layer

Figure 13 shows the relationship between the damping ratio obtained from the ARX model and the SI on the top floor. For the classroom and research buildings, the color of the plots is changed for each period, as in Fig. 10. For both buildings, the damping ratio between the top of the seismic isolation layer and the top floor is generally 0.02, which is the usual value for the design of steel structured buildings and high-rise buildings²¹⁾, and 0.05, indicating a little correlation with the SI. On the other hand, the damping ratios between the bottom of the seismic isolation layer and the top floor show a correlation with SI, except for 111/005 (CH2) on the south side of the research building, which tends to be larger than the damping ratio between the top of the seismic isolation layer and the top floor. During the Tohoku Earthquake, the damping ratio between the bottom of the base isolation layer and the top floor was large, which ranged from 0.10 to 0.40, confirming the damping effect of the base isolation members during strong ground motions. However, unlike the natural period, no clear change is observed in the relationship between the damping ratio and SI before and after the Tohoku Earthquake, which is consistent with previous studies^{6-8), 10)}.

On the other hand, in the CH1 direction of the multi-activity building, the damping ratio between the bottom of the seismic isolation layer and the top floor tends to be larger than that between the top of the seismic isolation layer and the top floor. In the CH2 direction, the damping ratio between the top of the seismic isolation layer and the top floor is also as large as that between the bottom of the seismic isolation layer and the top floor.

In common with the three buildings, even when a correlation is found between the damping ratio and the SI, the variation is larger than that of the natural period. This can also be confirmed in references 6–8 and 10 and is considered to be a limitation of the accuracy of the identification method itself.

6. CONCLUSION

Long-term vibration and earthquake observations were made on base-isolated irregular shaped buildings. Spectral analysis of microtremor records was conducted to examine the changes in the natural period over time at the microtremor level. The ARX model was then applied to the seismic records to evaluate the amplitude-dependent characteristics of the natural period and damping ratio during earthquakes. The conclusions obtained are listed below.

1. The natural period estimated from the spectral analysis of the long-term microtremor record at the corner of the top floor of each building showed seasonal variations and a negative correlation between the natural period and the temperature. The range of this variation was approximately 1%–3% of the average value of the natural period in previous years.
2. Comparison of the average natural period at the beginning of March just before the Tohoku Earthquake and the average natural period at the beginning of March in each year from 2012 to 2019 indicates that the Tohoku Earthquake caused a 4%–6% elongation of the natural period in the classroom and research buildings. This elongation is considered to be due to a slight decrease in building stiffness caused by damage to nonstructural members.
3. The relationship between the maximum acceleration of the seismic records of the upper and lower seismic isolation layers and the top floor showed that almost no change was found in the response relationship before and after the Tohoku Earthquake. This is because the Tohoku Earthquake did not damage the structural members and seismic isolation members.
4. The natural period estimated by applying the ARX model to the seismic records on the top and bottom of the seismic isolation layer and on the top floor correlated well with the SI (logarithmic value) on the top floor, confirming the amplitude dependence of the natural period. The regression equations between the natural period and SI obtained for the two time periods before and after the Tohoku Earthquake indicate that the natural period elongation is approximately 6%–10% for SI of 3 cm/s.
5. In many cases, the natural period during the Tohoku Earthquake was located above the regression equation between the natural period and SI obtained from the seismic record before the Tohoku Earthquake, which was consistent with the occurrence of damage to the nonstructural components of the building.
6. Comparison of the spectra of the top floor by weak earthquakes and microtremors and the transfer function (between the bottom of the seismic isolation layer and the top floor) during weak earthquakes indicates that the natural period estimated from the microtremors is that of the structure above the bottom of the seismic isolation layer.
7. Amplitude dependence was observed for the damping ratio between the bottom of the base isolation layer and the top floor. Unlike the natural period, the relationship between the damping ratio and SI did not change before and after the Tohoku Earthquake.

ACKNOWLEDGMENT

The authors would like to thank Dr. Nishikawa Takafumi of Nagasaki University, Mr. Ishii Seiji of Tokyo Sokushin Corporation, Mr. Kawaguchi Hideki of the Facilities Division of Shibaura Institute of Technology, and graduate students of the Earthquake Disaster Mitigation Laboratory, Shibaura Institute of Technology for their cooperation in the earthquake and continuous vibration observation. The observation system was partially supported by the Strategic Research Program of the Japan Science and Technology Agency (JST) in the area of advanced integrated sensing technology (CREST) under the title ‘Risk Monitoring and Disaster Management of Urban Infrastructure’ (principle investigator: Yozo Fujino). We also thank the reviewers and editorial board members for their valuable comments and suggestions. We would like to express our gratitude to them. The authors would like to thank Enago (www.enago.jp) for the English language review.

REFERENCES

- 1) Okamoto, Y., Akazawa, T., Yamada, M., Onishi, Y. and Hayashi, Y.: System Identification of the Vibration Characteristics for a High-Rise Building Using Continuous Seismic Records, *The AIJ Journal of Technology and Design*, Vol. 19, No. 41, pp. 59–84, 2013 (in Japanese).
- 2) Shiraishi, M., Saito, T. and Mita, A.: Local Damage Detection of a 3 Dimensional Structure Based on ARX Model of Substructures, *The AIJ Journal of Technology and Design*, Vol. 20, No. 44, pp. 55–60, 2014 (in Japanese).
- 3) Hatayama, T., Wang, X., Ohno, S. and Motosaka, M.: Change of Natural Frequency of Low Rised Buildings Based on Long-Term Vibration Records, *Journal of Japan Association for Earthquake Engineering*, Vol. 17, No. 4, pp. 1–12, 2017 (in Japanese).
- 4) Saito, T.: Changes in Dynamic Characteristics of a Seismically Isolated Building Caused by the 2011 off the Pacific Coast of Tohoku Earthquake, Shimizu Institute of Technology, *Technical Research Report*, Vol. 89, pp. 13–21, 2012 (in Japanese).
- 5) Kanazawa, K.: Diurnal Fluctuation Mechanism of Natural Frequencies of a Concrete-Made Building, *Journal of Structural Construction Engineering (Transactions of AIJ)*, No. 612, pp. 63–71, 2007 (in Japanese).
- 6) Shinohara, T., Kazama, H. and Harada, H.: The Seismic Records of the NIKKEN SEKKEI Tokyo Building Struck by the 2011 off the Pacific Coast of Tohoku Earthquake: Part 2: Overall Evaluation of the Records from April, 2003 to February, 2012, *Summaries of Technical Papers of Annual Meeting, Architectural Institute of Japan, Structure II*, pp. 1151–1152, 2012 (in Japanese).
- 7) Kashima, T., Koyama, S., Azuhata, T. and Inoue, N.: Change in Dynamic Characteristics of Super High-Rise Buildings Due to the 2011 Great East Japan Earthquake, *The AIJ Journal of Technology and Design*, Vol. 21, No. 48, pp. 493–497, 2015 (in Japanese).
- 8) Kashima, T.: Study on Changes in Dynamic Characteristics of High-Rise Steel-Framed Buildings Based on Strong Motion Data, *Procedia Engineering*, Vol. 199, pp. 194–199, 2017.
- 9) Konno, K., Nishikawa, T. and Fujino, Y.: Estimation of Lateral and Rotational Vibrations of a Base-Isolated Building during the 2011 Great East Japan Earthquake, *Journal of Japan Association for Earthquake Engineering*, Vol. 13, No. 3, pp.14–29, 2013 (in Japanese).
- 10) Siringoringo, M. D. and Fujino, Y.: Seismic Response Analyses of an Asymmetric Base-Isolated Building during the 2011 Great East Japan (Tohoku) Earthquake, *Structural Control and Health Monitoring*, Vol. 22, pp. 71–90, 2015.
- 11) Shibaura Institute of Technology: *Toyosu Campus Making Architecture*, 89 pp., 2008 (in Japanese).
- 12) Earthquake Disaster Mitigation Laboratory, Shibaura Institute of Technology: Earthquake Observation at Shibaura Institute of Technology Toyosu Campus (Base-Isolated Structures) (in Japanese). <http://www.eq.db.shibaura-it.ac.jp/Mensin/index.shtml> (last accessed on June 18, 2023)
- 13) Nishikawa, T., Konno, K., Fujino, Y. and Nakayama, M.: High-Density Structural Health Monitoring System for High-Rise Seismic Isolated Building Using Existing Network Facilities, *Journal of Japan Association for Earthquake Engineering*, Vol. 14, No. 2, pp. 1–15, 2014 (in Japanese).
- 14) Japan Meteorological Agency: Past Climate Data Search (in Japanese, title translated by the authors). <https://www.data.jma.go.jp/obd/stats/etrn/index.php> (last accessed on June 18, 2023)
- 15) Şafak, E.: Adaptive Modeling, Identification, and Control of Dynamic Structural Systems 1: Theory, *Journal of Engineering Mechanics*, Vol. 115, No. 11, pp. 2386–2405, 1989.
- 16) Saito, T.: System Identification of a High-Rise Building Applying Multi-Input-Output ARX Model of Modal Analysis, *Journal of Structural Construction Engineering (Transactions of AIJ)*, No. 508, pp. 47–54, 1998 (in Japanese).
- 17) Earthquake Disaster Mitigation Laboratory, Shibaura Institute of Technology: List of Earthquakes (in Japanese). http://www.eq.db.shibaura-it.ac.jp/Mensin/EQ_LIST/EQ_LIST.pdf (last accessed on June 18, 2023)
- 18) Japan Meteorological Agency: Seismic Intensity Database Search (in Japanese, title translated by

the authors). <https://www.data.jma.go.jp/svd/eqdb/data/shindo/index.html> (last accessed on June 18, 2023)

- 19) Adachi, S.: *System Identification for Control Using MATLAB*, Tokyo Denki University Press, 202 pp., 1996 (in Japanese).
- 20) Yamamoto, G., Fujita, S., Harada, H., Nakamizo, D., Minagawa, K. and Iyama, Y: Construction of Vibration Analysis Model of Tokyo Denki University Building No. 1 Considering Amplitude Dependence Based on Seismic Records, *Journal of Japan Association for Earthquake Engineering*, Vol. 18, No. 1, pp. 89–103, 2018 (in Japanese).
- 21) Architectural Institute of Japan: *Guidebook of Recommendations for Loads on Buildings*, Architectural Institute of Japan, 506 pp., 2016 (in Japanese).

(Original Japanese Paper Published: August, 2021)

(English Version Submitted: July 27, 2023)

(English Version Accepted: November 11, 2023)